A single residue deletion in the barley HKT1;5 P189 variant restores plasma membrane localisation but not Na^+ conductance

Wege, Stefanie; Qiu, Jiaen; Byrt, Caitlin; Houston, Kelly; Waugh, Robbie; Gilliham, Matthew

Published in:
BBA - Biomembranes

DOI:
10.1016/j.bbamem.2021.183669

Publication date:
2021

A single residue deletion in the barley HKT1;5 P189 variant restores plasma membrane localisation but not Na+ conductance

Stefanie Wege, Jiaen Qiu, Caitlin Byrt, Kelly Houston, Robbie Waugh, Matthew Gilliham, Maria Hrmova

PII: S0005-2736(21)00119-X

DOI: https://doi.org/10.1016/j.bbamem.2021.183669

Reference: BBAMEM 183669

To appear in: *BBA - Biomembranes*

Received date: 25 February 2021

Revised date: 1 June 2021

Accepted date: 2 June 2021

Please cite this article as: S. Wege, J. Qiu, C. Byrt, et al., A single residue deletion in the barley HKT1;5 P189 variant restores plasma membrane localisation but not Na+ conductance, *BBA - Biomembranes* (2018), https://doi.org/10.1016/j.bbamem.2021.183669

A single residue deletion in the barley HKT1;5 P189 variant restores plasma membrane localisation but not Na^+ conductance

Stefanie Wege [a,b,#], Jiaen Qiu [a,b,#], Caitlin Byrt [b,c], Kelly Houston [d], Robbie Waugh [a,d,e], Matthew Gilliham [a,b], Maria Hrmova [f,a *]

[a] School of Agriculture, Food and Wine, and Waite Research Institute, University of Adelaide, Waite Research Precinct, Glen Osmond, SA 5064, Australia

[b] ARC Centre of Excellence in Plant Energy Biology, Waite Research Institute, University of Adelaide, Waite Research Precinct, Glen Osmond, SA 5064, Australia

[c] Research School of Biology, The Australian National University, Canberra, ACT 2601, Australia

[d] Cell and Molecular Sciences, The James Hutton Institute, Errol Road Invergowrie, Dundee, DD2 5DA, Scotland, UK.

[e] School of Life Sciences, University of Dundee, Dow Street, Dundee, DD1 5EH, Scotland, UK

[f] School of Life Science, Huaiyin Normal University, Huai'an 223300, China

[#]These authors contributed equally.

*Corresponding author; *E-mail address*: maria.hrmova@adelaide.edu.au (MH).

Abstract

Leaf Na^+ exclusion, mediated by plasma membrane-localised Class 1 High-affinity potassium (K^+) Transporters (HKTs), is a key mechanism contributing to salinity tolerance of several major crop plants. We determined previously that the leucine to proline residue substitution at position 189 (L189P) in barley HvHKT1;5 disrupts its characteristic plasma membrane localisation and Na^+ conductance. Here, we focus on a surprising observation that a single residue deletion of methionine at position 372 (M372del) within the conserved VMMYL motif in plant HKTs, restores plasma membrane localisation but not Na^+ conductance in HvHKT1;5 P189. To clarify why the singular M372 deletion regains plasma membrane localisation, we built 3D models and defined α-helical assembly pathways of the P189 M372del mutant, and compared these findings to the wild-type protein, and the HvHKT1;5 L189 variant and its M372del mutant. We find that α-helical association and assembly pathways in HvHKT1;5 proteins fall in two contrasting

categories. Inspections of structural flexibility through molecular dynamics simulations revealed that the conformational states of HvHKT1;5 P189 diverge from those of the L189 variant and M372del mutants. We propose that M372del in HvHKT1;5 P189 instigates structural rearrangements allowing routing to the plasma membrane, while the restoration of conductance would require further interventions. We integrate the microscopy, electrophysiology, and biocomputational data and discuss how a profound structural change in HvHKT1;5 P189 M372del impacts its α-helical protein association pathway and flexibility, and how these features underlie a delicate balance leading to restoring plasma membrane localisation but not Na^+ conductance.

Keywords: 3D protein modelling; α-helical association and assembly pathways; confocal microscopy; molecular dynamics simulations; salinity; two-electrode voltage-clamp.

Abbreviations: 3D, three dimensional; CBL1n, calcineurin B- like protein 1n; CHARMM, Chemistry at Harvard Macromolecular Mechanics; DOPE, Discrete Optimised Protein Energy function; DSS, Database of Secondary Structure; GFP, Green Fluorescent Protein; HAP, haplotype; HKT, High-affinity potassium (K^+) Transporter; Hv, *Hordeum vulgare*; KtrB, K^+ transporter (Trk) protein B; MD, molecular dynamics; MEME, Multiple EM (Expectation Maximization) for Motif Elicitation; PDB, Protein Data Bank; RFP, Red Fluorescent Protein; RMSD, Root Mean Square Deviation; RMSF, Root Mean Square Fluctuation; TEVC, Two-Electrode Voltage-Clamp.

1. Introduction

Sub-soil constraints including low water availability, nutrition, extreme pH values, or the presence of elements that can be toxic to plants if they accumulate to high cellular levels are major limitations to global crop yields. Cellular elemental transport is mediated by membrane-embedded transporters that control exclusion, exudation, or compartmentation of mineral elements across cellular membranes to facilitate adequate nutrition, signalling and developmental processes and safeguard against toxicity [1-3]. High soil sodium chloride or salinity (elevated Na^+ and Cl^- concentrations) interfere with cell expansion, photosynthetic activity, and can cause leaf senescence and reductions in reproductive capacity when accumulated in cells [4-7]. Na^+ is

considered to be a non-essential element for the growth and development of most plants, although some plants benefit from high intracellular Na^+ concentrations when the essential K^+ level in the soil is low [8].

Despite the sequencing of multiple crop genomes and obtaining structural information in some transporters, relatively few transport proteins have been characterised at physiological, biochemical, and structural levels. This is because whole-genome sequencing and well-annotated functional genomic data are scarce, and without the transporters being isolated, characterised, and linked with protein dynamics, their precise functional data cannot be obtained [3,9,10].

Here, we focus on the High-affinity potassium (K^+) Transporter (HKT) integral membrane proteins that occur exclusively in plants but have bacterial and fungal orthologues in the KtrB/TrK/ TrG/KdpA/HKT superfamily of cation transporters [11-13], which share similar structural folds [14-16]. Plant HKT transporters occurring in multiple genera and are believed to permeate predominantly monovalent cations [17-19], although HKTs conducting Mg^{2+} and Ca^{2+} were reported [20-21]. Plant HKTs form two groups based on their transport selectivity: (i) class 1 are Na^+ uniporters, and (ii) class 2 conduct Na^+ and K^+ (and potentially the symport of both ions) and are uniporters of Na^+ at high concentrations [22].

Natural sequence variations of transport proteins at single or multiple residues are useful tools for examining the functional relationships bestowed by specific residues, where a transporter can lose function, change selectivity, and have modified transport rates or other properties [8,19,23,24]. However, it is impossible to prove the exact molecular mechanism that underlies functional changes of transporters by examining a sequence alone, unless conducting multidisciplinary analyses. Examples of such approaches include research on *HKT1;5* genes and corresponding gene products in wheat [24-26] and barley (*Hordeum vulgare, Hv*) [8]. In the barley study [8], grain Na^+ across a genome-wide association panel was quantified and variants of a class 1 *HKT1;5* responsible for Na^+ content variation under non-saline conditions were identified. These authors also identified a leucine to proline substitution at position 189 (L189P) in HvHKT1;5 that disturbed its characteristic plasma membrane localisation and disrupted Na^+ transport – this variation was also described at the protein structural level [8]. Barley genotypes

that contained HvHKT1;5 variants with L189 had low levels of Na^+ (haplotypes Na^+_{HAP1} and Na^+_{HAP2}), while P189 variants (haplotype Na^+_{HAP3}) have higher Na^+ levels [8]. Similarly, Borjigin et al. [25] found the causal variation underlying a sixfold higher leaf and sheath Na^+ content in a Portuguese wheat landrace compared to the Australian Gladius and Scout wheat cultivars. In a Portuguese landrace, this was a naturally occurring L190P variation in the TaHKT1;5-D Na^+ transporter with a significant structural impact. These studies provide the information that would allow considerations of the fundamental complexities underlining transport function, *i.e.* how residues in a protein interact together in a structural context, and with solutes to facilitate transport. For this to be fully realised, a transporter needs to be resolved at an atomic level and dynamically understood [3,9]. In crop transporters, the significance of such approaches is emerging and is being used to deliver crop improvements through biotechnological applications [1,23,27].

In the present study, we further assessed the structure-function relationships of HvHKT1;5 proteins. We used comparative bioinformatics analyses *via* ConSurf [28] and Multiple EM (Expectation Maximization) for Motif Elicitation (MEME) [29] of plant HKT transporters and bacterial Ktr (that are orthologues of plant HKT transporters). We identified a highly conserved VMMYL motif (residues 371-375) in plant HvHKT1;5 transporters that was not up till now characterised, and that corresponded to the conserved LLMFI motif in bacterial Ktr proteins. Given the high evolutionary conservation scores of Met372 and Met373 in the VMMYL motif of plant HKTs (and corresponding Leu300 and Met301 in the LLMFI motif of bacterial orthologues), we were interested in the impact of a single deletion M372 (M372del) in barley HvHKT1;5 transporters. We generated M372del mutants (by removing M372 to generate the V-MYL motif) in Na^+_{HAP1} (HvHKT1;5 L189) and Na^+_{HAP3} (HvHKT1;5 P189) variants. We arrived at the surprising observation that M372del in the barley HvHKT1;5 P189 restored its plasma membrane localisation but prevented Na^+ conductance. We conducted comparative confocal microscopy, electrophysiology, and biocomputational analyses of HvHKT1;5 L189 and P189 proteins and their M372del mutants to rationalise our observation that M372del in P189 leads to regaining of plasma membrane localisation (contrary to the P189 variant) with the aim to resolve how structural changes in the context of L189 or P189 variations, and M372 deletions in HKT transporters impact protein tertiary morphogenesis or topogenesis.

2. Materials and methods

Accession numbers of HvHKT1;5 sequences

National Center for Biotechnology Information (Bethesda, MD, USA) accessions of HvHKT1;5 proteins are as follows: Golden Promise (haplotype Na^+_{HAP1}; L189; MT334697), Viivi (Na^+_{HAP2}; L189; MT312249), and Morex (Na^+_{HAP3}; P189; MT334696).

Structural bioinformatics analyses of plant HKT and bacterial Trk sequences

Analyses of conservation of amino acid residues were conducted *via* ConSurf [28] and motifs distributions analyses were performed *via* Multiple EM (Expectation Maximization) for Motif Elicitation (MEME) [29] in 26 plant HKT and 26 bacterial Trk transporters (Supplementary Data Set 1, Supplementary Fig. 1). All multiple sequence alignments shown in Supplementary Data Set 1 were implemented in Clustal Omega [30]. To highlight sequence differences in HvHKT1;5 from Golden promise (Na^+_{HAP1} haplotype; L189), Viivi (Na^+_{HAP2}; L189), and Morex (Na^+_{HAP3}; P189) cultivars, the sequences were aligned in PROMALS3D [31] (Supplementary Fig. 2).

Subcellular localisation of HvHKT1;5 L189 and P189, and M372del mutant proteins through transient expression in tobacco (**Nicotiana benthamiana L.**) *leaf epidermal cells*

Subcellular localisation was performed according to Wu et al. [32]. Briefly, coding sequences of variant and M372del mutant proteins were shuttled into the pMDC43 expression vectors to generate NH_2-terminally Green Fluorescent Protein (GFP) GFP-tagged HKT1;5 proteins, with gene expression driven by the 2x35S promoter. The free cytosolic GFP protein was expressed as described [32]. A twelve-residue peptide from the *Arabidopsis* calcineurin B- like protein (CBL1n) was used as a plasma membrane marker, tagged NH_2-terminally to Red Fluorescent Protein (RFP) [33]. For tobacco infiltration, *Agrobacterium tumefaciens* harbouring the two constructs were combined into a plasmid with the p19 suppressor of gene silencing to maximise expression [32]. Leaves were imaged two days after infiltration, using a Nikon A1R confocal laser scanning microscope and the NIS-Elements C software (Nikon Corporation, Minato, Tokyo, Japan). GFP signals were imaged using the 488 nm excitation wavelength, and the 500–

550 nm bandpass filter to capture GFP emission, whilst RFP was imaged using the 561 nm excitation wavelength and the 570–620 nm bandpass filter to capture RFP emission. Images were prepared and assembled in ImageJ [34]. 3D animation of the GFP-HvHKT1;5 P189 and RFP-CBL1n image-stack is composed of 52 single images, with a step size of 0.3 µm, and has a total depth of 15.4 µm (Supplementary Video 1.avi); this video can be played with a standard VLC Media Player.

Characterisation of HvHKT1;5 L189 and P189, and their M372del mutant proteins in **Xenopus laevis** *oocytes*

Methods for functional characterisation of HvHKT1;5 variant and mutant proteins were as described previously [8,26,35]. Briefly, nucleotide sequences of variants and mutants were synthesised by GenScript (Piscataway, NJ, USA), and DNA sequences were inserted into a Gateway enabled pGEMHE vector. pGEMHE constructs were linearised using sbfI (New England Biolabs, Massachusetts, USA) and complementary RNAs (cRNAs) were transcribed using the Ambion mMESSAGE mMACHINE kit (Life Technologies, Carlsbad, CA, USA). cRNA (23 ng in 46 nL of RNA-free water) or equal volumes of RNA-free water were injected in oocytes, followed by incubations in ND-96 for 24–48 h before measurements. Currents were recorded in the HMg solution as described [8]. Solution osmolarities were adjusted using mannitol at 220–240 mOsmol kg^{-1} [26].

Construction of 3D models of HvHKT1;5 M372del mutant proteins in complex with Na^+

The KtrB K^+ subunit (Protein Data Bank ID 4j7c, chain I) of the KtrAB transporter from *B. subtilis* [16] was used as a template for 3D structural modelling of HvHKT1;5 L189 M372del and P189 M372del mutants, as described [8,24-26]. The KtrB K^+ structure has the K^+ ion in the selectivity filter that was substituted by Na^+ in HvHKT1;5 models, as the barley transporter permeates this ion at a faster rate than K^+ [8]. 3D structural models of L189 M372del and P189 M372del mutants in complex with Na^+ with ionic radii taken from CHARMM [36,37] were generated using the Modeller 9v19 platform [38] under the Fedora 12 operating system. In each case, a total of 50 models was built and scored by the Modeller 9v19 objective function [39], the Discrete Optimised Protein Energy function (DOPE) [40], PROCHECK [41], ProSa 2003 [42], QMEAN6 [43], and FoldX [44] – final molecular models were selected based on the most

favourable combination of scoring parameters. Evaluations of Gibbs free energy differences of L189 M372del and P189 M372del mutants ($\Delta\Delta G = \Delta G_{mutant} - \Delta G_{wild\text{-}type}$) were performed in FoldX [44] and cavity volumes were calculated with CASTp [45]. Structural images were drawn in PyMOL Molecular Graphics System v2.3.3 (Schrődinger LLC, Portland, OR, USA). Root Mean Square Deviation (RMSD) values were calculated in PyMol *via* the sequence-independent structure-based dynamic programming alignment algorithm based on Cα atoms.

Evaluations of stereo-chemical parameters indicated that L189 M372del and P189 M372del models had 99.5% and 99.7% residues in allowed regions and two (0.5%) and three (0.7%) residues in disallowed regions (except Gly and Pro), respectively. Average G-factors (measures of the correctness of dihedral angles and main-chain covalent bonds) of L189 M372del and P189 M372del calculated by PROCHECK were -0.14, and -0.03, respectively, and ProSa 2003 z-scores (measures of Cβ-Cβ pair interactions) were -5.6, and -5.5, respectively. QMEAN6 normalised score values of L189 M372del and P189 M372del (a linear combination of six descriptors that are independent of a sequence length) were 0.477 and 0.519, respectively; the values between 0-1 are indicative of high-quality models when X-ray crystallography-derived templates are used for model calculations [43]. The listed evaluation parameters indicated that L189 M372del and P189 M372del models satisfied stereochemical parameters and were satisfactory.

Predictions of transmembrane α-helical association (folding) pathways of HvHKT1;5 variant proteins and their M372del mutants

Calculations of energies in pairwise structurally associated α-helical regions and protein folding pathways of polytopic L189 and P189 models, and L189 M372del and P189 M372del mutants were performed in TMPfold [46]. Compared to our earlier work [8], where the topology of HvHKT1;5 taken from PolyPhobius [47], in this work we extended the number of α-helices defined by the Database of Secondary Structure (DSS) algorithm implemented in PYMOL (DSS defines secondary structures based on the backbone geometry and hydrogen bonding patterns) and excluded those that were equal or less than three residues in length. The TMPfold analysis (based on analyses of known 3D structures) returns: (i) pairwise energies of association of membrane helices; (ii) total energy of association for all membrane α-helices in a subunit; (iii)

pairwise energies of association of all membrane subunits in a multiprotein complex; and (iv) the total energy of association of all subunits in the protein. Based on these limits, TMPfold suggests a tentative folding pathway and sequence of folding intermediates for a membrane protein structure, where an α-helical assembly could be initiated from the formation of strongly interacting pairs of sequential α-helices [α-hairpins] that form folding nuclei [48].

Molecular dynamics (MD) simulations of HvHKT1;5 variant proteins and their M372del mutants

MD simulations (four runs for each system with data averaging) using CABS-flex 2.0 [49] used the following settings and restraints (mode: regular secondary structures; gap: 3 residues; minimum distance: 3.8 Å; maximum distance: 8.0 Å; temperature: 1.4-dimensionless; length: 200 nsec) were used. Simulation runs were based on initial conformation inputs taken from 3D models to determine Root Mean Square Fluctuation (RMSF) values (defined as a measure of the displacement of Cα atoms, relative to Cα atoms of the reference structure over simulation time) to establish how relative propensities of residues deviate from the dynamics of an average HvHKT1;5 structure. MD parameters optimized by all-atom simulations aim to provide the best possible convergence between CABS-flex MD simulations and consensus fluctuations, whereby the fully statistical knowledge-based force field considers solvent effects that are incorporated implicitly [49]. Input 3D models were used as starting points for MD simulations and resulting trajectories were analysed to describe protein dynamics based on 1,000 models clustered in ten representative all-atom medoids of each class; data are presented in Figs. 4 and 5.

3. Results

Identification of VMMYL motifs in plant HKT, and LMFI motifs in bacterial Trk sequences

Comparative structural bioinformatics analyses of plant HKT and bacterial Trk sequences through ConSurf [28] and MEME [29] revealed high evolutionary conservation scores for Met372 and Met373 in the VMMYL motif (residues 331-335) (P-value of the peptide motif with VMMYL is $2.7e^{-327}$) in HvHKT15 L189 and P189 cultivars (Supplementary Figs. 1 and 2). The corresponding Leu300 and Met301 in the LLMFI motif (residues 299-303) (P-value of the peptide motif with LLMFI is $4.9e^{-307}$) in *B. subtilis* KtrAB had also high conservation scores

(Supplementary Data Set 1, Supplementary Fig. 1). Given the high conservation of both motifs and absolute conservation of M373 or M301 in respective plant and bacterial transporters, we examined the role of Met372 in barley HKT1;5 L189 and P189 variants. We generated M372del mutants (by removing a single M372 to generate the V-MYL motif) in Na^+_{HAP1} (HvHKT1;5 L189) and Na^+_{HAP3} (HvHKT1;5 P189) variants, inspected their biological (plasma membrane localisation and permeation function) and biocomputational (structures, transmembrane α-helical association – folding pathways and molecular dynamics) characteristics, and compared to those of HvHKT1;5 L189 and HvHKT1;5 P189 variant proteins.

Transient co-expression of GFP-HvHKT1;5 variant and M372del mutant proteins with CBL1n-RFP plasma membrane marker in* Nicotiana benthamiana *leaf epidermal cells

We have shown previously that the NH_2-terminally GFP-tagged HvHKT1;5 L189 variant and the P189L mutant proteins localised to the plasma membrane, while the GFP-tagged P189 variant protein failed to do so when expressed in *Nicotiana benthamiana* epidermal cells [8]. Here, the GFP-HvHKT1;5 L189 variant protein also consistently localised to the plasma membrane of tobacco cells (Fig. 1A), as observed earlier [8]. Similar data were obtained for the L189 variant protein from the Viivi cultivar (Na^+_{HAP3} haplotype) (data not shown). However, the GFP-tagged P189 mutant did not co-localise with the plasma membrane marker and its GFP-signal pattern was present in most cells in bright immobile structures, which typically indicate protein aggregates or inclusion bodies (Fig. 1B, Supplementary Video 1). In other tobacco cells, the GFP signal of this protein was visible in the endoplasmic reticulum, indicating that GFP-HvHKT1;5 was retained in this organelle, and sometimes we also detected bright immobile structures resembling proteasomes (Supplementary Fig. 2). In this regard, we were interested to find out, if mutants of the P189 variant could be routed to the plasma membrane *via* mutations or deletions. To this end, we created M372del mutants, where M372 residues were deleted in both L189 and P189 HvHKT1;5 transporters. The GFP-tagged L189 M372del mutant showed the same plasma membrane localisation pattern as the wild-type L189 protein, it was derived from (Fig. 1C), however, strikingly, the P189 M372del mutant protein was also routed to the plasma membrane (Fig. 1D). In the latter case, we did not observe protein degradation patterns that were typical for GFP-HvHKT1;5 P189, as this P189 M327del protein consistently co-localised with the RFP-CBL1n plasma membrane marker (Fig. 1D). Notably, the GFP-signal patterns of all GFP-

HvHKT1;5 variant proteins differed from those of cytosolic free GFP, which localised to the thin layer of cytosol close to the plasma membrane, and inside and around the nucleus (Supplementary Fig. 3).

Transport of Na^+ and K^+ by HvHKT1;5 L189 and M372del variant proteins

Our earlier data indicated that a single substitution in the HvHKT1;5 P189 protein disrupts its function *in planta* and when heterologously expressed in oocytes, while the P189L mutant of the same variant protein or the L189 protein, facilitated Na^+ transport [8]. In this work, we confirmed these data using Two-Electrode Voltage-Clamp (TEVC) (Figs. 2A and 2B). Given that both GFP-tagged HvHKT1;5 P189 M372del and L189 M372del localised to the plasma membrane (Figs. 1C and 1D), we were able to investigate if the artificial deletion of M372del was deleterious to transport function, or if transport can be restored through this deletion that returned plasma membrane localisation of the HvHKT1;5 P189 M372del protein. We, therefore, tested the L189 M372del and P189 M372del mutant proteins after their expression in *Xenopus laevis* oocytes using TEVC. During these measurements, the oocytes that were injected with cRNA of HvHKT1;5 L189 showed significant inwards currents in the presence of external Na^+ (1 and 30 mM) or small currents in the presence of external K^+ (30 mM) (Fig. 2A). However, the oocytes injected with cRNA of P189, P189 M372del, and L189 M372del did not facilitate any significant currents (Figs. 2B, 2C, and 2D). Since the conductance of both M372del mutants remained at a control water-injected level (Fig. 2E), we concluded that monovalent ion transport function was compromised in HvHKT1;5 M372del mutants.

3D models of HvHKT1;5 M372del variant proteins in complex with Na^+

To explore the implications of M372 deletions in orthologous L189 M372del and P189 M372del mutants at a structural level, we constructed their 3D molecular models in complex with Na^+ using the *B. subtilis* KtrB K^+ transporter (Protein Data Bank ID 4j7c, chain I) as a template [16,24,26] (Fig. 3). Analyses of 3D models of these mutants and specifically the environments of α-helices 6 (carrying L189 and P189) and α-helices 12 (carrying M372 deletions), indicated that there were differences in tilting angles between α-helices 6 and 7, due to the L189 or P189 change [8]. Comparisons of HvHKT1;5 L189 and P189 M372del mutants indicated that M372 deletions did not substantially change angular parameters of α-helices 12 (Fig. 3C), but that the

residues within α-helices 12 in the regions of M372 deletions faced different environments. To this end, residues within the VMMYL motifs of wild-type proteins recognised V368, V369, M370, and V417 side-chains in their vicinity, compared to the residues of V-MYL motifs that interacted with R349, V368, and V416 side-chains in M372del mutants (Figs. 3A and 3B).

Guo et al. [50] showed that during membrane protein folding, the volumes of protein central cavities affect the packing of α-helices and the morphogenesis of tertiary structures, also known as topogenesis, and that substantially changed central cavity volumes disturb these processes. Central cavity volumes assessments [45] of HvHKT1;5 L189 and P189 and their M372del mutants pointed to significant differences in their volumes (930 Å^3 and 1,407 Å^3 in L189 and P189, respectively), while the central cavity volumes in L189 M372del (986 Å^3) and P189 M372del (1,055 Å^3) were comparable and similar to that of L189.

Evaluations of total Gibbs free energy values of HvHKT1;5 L189 and P189 proteins and their M372del mutants revealed destabilising energy values of $\Delta\Delta G$ = +62 kcal/mol and $\Delta\Delta G$ = +48 kcal/mol, respectively, indicating that the M372 deletion was more disruptive in the P189 variant. Assessments of the Gibbs free ΔG energy differences in L189 M372del showed that the L189P mutation was energetically highly destabilising with ΔG = +6.6 kcal/mol, while the conversion of other five small, polar or aliphatic residues (S57, Q102, N131 I416, N438) to those of HvHKT1;5 P189 M372del (N57, E102, K131 V416, S438) resulted in the low destabilising energy of ΔG = +0.7 kcal/mol.

Predictions of transmembrane α-helical association (folding) pathways of HvHKT1;5 variant proteins and their M372del mutants

We used TMPfold [46] to predict tentative transmembrane α-helical association or folding pathway parameters in HvHKT1;5 variants and their M372del mutant proteins, where the folding pathways or equations are calculated based on: (i) transmembrane α-helices are inserted into a membrane sequentially; (ii) each α-helix is added in a separate step; (iii) newly synthesised α-helix associates stably with a previous α-helix or a nucleus (defined as an assembly of sequentially adjacent α-helices); and (iv) sequentially adjacent structures associate first. Evaluations of tentative folding pathways of HvHKT1;5 proteins and M372del mutants and the

template crystal structure KtrB K^+ indicated that these equations differed in L189, and P189 and L189P HvHKT1;5 variant, and M372 deletion mutant proteins (Table 1 and Supplementary Table 1). The analysed protein folding pathways fell into two main categories (Table 1 and Supplementary Table 1): (i) the KtrB K^+ template, L189 and L189 M372del and P189L proteins folded through three separate steps, where folding of nuclei of α-helices 1-7, 8-13 and 14-17 (KtrB K^+), or 1-4-5, 5-6-9-10, 11-of 12-17 (L189, P189L, and L189 M372del) occurred in three independent events *via* 1-14 individual steps. (ii) In P189, and P189 M372del proteins, this pathway was altered, with proteins folding similarly, where all 17 α-helices folded in succession in one event through 1-16 steps. Here, a nucleus of 1-5 α-helices folded together, while α-helices 6 (containing P189 variation or P189L mutation) folded together with α-helix 7, and α-helices 12 (containing M372 deletions) folded separately with α-helices 9-11 and 13-17. Notably, there were four steps required in the folding pathway required for P189 that involved α-helix 6, while five of those were needed for P189 M372del (Supplementary Table 1). We also looked at the folding pathway of the L189P mutant, as we previously showed that this mutant was routed to the plasma membrane, contrary to P189 [8]. Indeed, upon implementing the P189L mutation, this transporter followed the same folding pathway as the L189 variant protein (Supplementary Table 1).

Structural dynamics of HvHKT1;5 variant proteins and their M372del mutants

The aim of MD simulations utilising CABS-flex 2.0 [49] was to look into the local and global flexibility of HvHKT1;5 L189 and P189 proteins and their M372 del mutants, and into the differences in flexibility between these protein pairs. We analysed protein dynamics over 200 nsec of converged simulation runs (Supplementary Fig. 4) by charting RMSF values (or averaged RMSD values over simulation time) (Figs. 4 and 5) and looked at residues that oscillated or were stable over MD simulation runs.

In examined HvHKT1;5 L189 and P189 proteins and their M372del mutants we observed that the flexibilities of loops adjoining α-helices 1-2, 2-3, 4-5, 5-6, α-helices 5-7, the loop adjoining α-helices 7-8, the loop adjoining α-helices 9-10, α-helices 11-13, and loops adjoining α-helices 14-15 and 15-16 showed 'peaks' in charts (Figs. 4 and 5; shown in all residue fluctuation plots). These RMSF peak values (up to 5 Å) were significantly above the average values in each

modelled structure, and suggested that the described structural elements exerted higher degrees of flexibility than the remainder of the structures, and that the flexibilities of these secondary structure elements may be correlated.

Further analyses of differences between RMSF values of the HvHKT1;5 L189 and P189 (Fig. 4), and HvHKT1;5 L189 M372del and P189 M372del (Fig. 5) protein pairs showed that these values of the L189 protein, in the 121-201 residue region (containing α-helix 6 with L189), fluctuated significantly more than those in the same region of the P189 protein, whereby some of these residues were fairly rigid (Fig. 4A). The region that contained α-helix 12 (residues 363-375) with VMMYL motifs (residues 371-375, coloured in cyan; Fig. 4B) and α-helix 13 (coloured in wheat; Fig. 4B, left panel) in L189 was also more flexible compared to the same region in P189 (Figs. 4A and 4B). The RMSF *versus* Cα atom plot (Fig. 4A) coincided with the superpositions of ten representative L189 and P189 models of variant proteins (Fig. 4B); here the former protein exhibited well-defined structural compactness compared to the P189 protein, where specifically α-helix 6 (coloured in magenta) and neighbouring α-helices 4 and 5 (coloured in wheat in L189; *cf.* Fig. 4B, left and right panels) were compacted less tightly.

Conversely, differences in the RMSF *versus* Cα atom plot of L189 M372del and P189 M372del mutants (Fig. 5A) showed that L189 M372 was more rigid in α-helix 6 that contained L189. The P189 M372del mutant with its increased flexibility in α-helix 6, also showed higher mobility in the loop region (coloured in wheat in Fig. 5B, right panel; residues 274-298) that adjoins α-helices 9 and 10. Further, α-helix 12 with M372del in the V-MYL motif (residues 371-374), the neighbouring α-helices 11 and 13, and the loop adjoining α-helices 14 and 15 (coloured in wheat in Fig. 5B, right panel; residues 428-434) were pronounceably (α-helices 11) or slightly (α-helix 13 and the loop adjoining α-helices 14 and 15) more flexible in P189 M372 (*cf.* Fig. 5, left and right panels). Flexibilities of α-helices were reflected in the superpositions of ten representative models with only somewhat different structural packing (Fig. 5B).

4. Discussion

Defining details of membrane protein folding as they emerge from a ribosome or an unfolded state is a longstanding challenge [51,52]. In prokaryotes, polytopic membrane protein insertions

happen mainly co-translationally [51], while in eukaryotes this occurs at an endoplasmic reticulum *via* elaborate pathways involving membrane protein insertase complexes [53], or *via* spontaneous insertion of nascent chains and translocon-unassisted folding [54]. Novel biocomputational approaches, such as TMPfold [46], are needed to evaluate the protein folding pathways of membrane proteins. Here, we used this approach together with 3D protein modelling and MD simulations to predict transmembrane α-helical assembly pathways of HvHKT1;5 proteins and their M372del mutants. The aim was to explain an unexpected observation in barley HvHKT1;5 that a single deletion of methionine at position 372 (M372del) in L189 (Na^+_{HAP1} haplotype in Golden promise cultivar) and P189 (Na^+_{HAP3} haplotype in Morex cultivar) proteins, caused plasma membrane routing but not Na^+ conductance. Similar data were obtained with L189 M372del (Na^+_{HAP2} haplotype in Viivi cultivar) that carries L189 (data not shown). These findings demonstrated that the P189 variation did not disrupt the plasma membrane localisation of P189 M372del, and that the M372del deletion served as a partial suppressor mutation, as it restored the plasma membrane localisation but not monovalent ion conductance. The key differences and summary of properties describing this remarkable observation are summarised in Table 2 and discussed below.

When considering L189 and P189 variations it needs to be emphasised that a proline residue (in a structural context) is known to increase protein rigidity in surrounding regions, due to the unique chemistry of this residue. Conversely, a single deletion in α-helices (such as M372 in HvHKT1;5 transporters) may lead to destabilisation, due to changes in how residues contribute to interactions; this prevents them from forming stable contacts in modified environments. Consequently, we observed significant differences in folding pathways between the L189 and P189, and their M372del mutant proteins, which might explain why L189 M372del and in particular P189 M372del localised to the plasma membrane contrary to the P189 protein. We found that assembly pathways of these proteins fell in two categories with subtle differences between the two groups, where HvHKT1;5 proteins with wild-type protein folding pathways (that proceed through three steps) localised to the plasma membrane, while the P189 protein with a modified folding pathway failed to do so (Table 1 and Supplementary Table 1). It is of note that there were subtle (but important) differences in folding pathways between P189 and its M372del mutant that could play key roles in protein stability and the reconstitution of plasma

membrane localisation (Supplementary Table 1). Here, four steps were required in the α-helical assembly pathways for P189 involving α-helix 6, while five steps were needed for P189 M372del. Further analyses of packing interactions that are critical driving forces in α-helical membrane protein folding [50] indicated that there were substantial differences in volumes of central cavities of L189 and P189 variant and M372del mutant structures. The volume of the central cavity of P189 was 33-51% larger than those of L189 and their M372del mutants, which were comparable. Guo et al. [50] showed that internal cavities facilitate lateral movements of proteins in membranes that may be compromised if these cavities are modified or unstable. These cavity accommodations serve as a platform to fine-tune the balance between protein stability and flexibility for plasma membrane localisation and optimal activity.

In-depth analyses of α-helical assembly and folding pathways were supplemented with protein local and global flexibility data obtained through MD simulations (Figs. 4 and 5). These data revealed that conformational states and dynamics of the HvHKT1;5 P189 transporter differed from those of L189 and both M372 mutants that shared similar properties – in other words, the flexibility of several structural parts of the P189 variant was compromised. The charting of RMSF values coincided with the characteristics of representative 3D models of L189 and P189 variant and M372del mutant proteins, that showed a defined or less defined structural compactness. Additionally, we observed the inter-linked changes in the dynamics of α-helices 4-6, and α-helices 12-13 in L189, compared to P189 (Fig. 4). We also observed similar changes in correlated movements of α-helices 11-13 and two loops adjoining α-helices 9-10 and 14-15 in the P189 M372del protein (Fig. 5), relative to L189 M372del. We suggest that these changes in the flexibility of α-helices and loops in the HvHKT1;5 P189 M372 protein could have been caused by the deletion of Met372. In this regard, α-helices 12 in wild-type proteins recognised different residues in their vicinity (Figs. 3A and 3B) and were tracked by two proline residues on a loop. Inevitably, shorter α-helices 12 in M372del mutants (Figs. 3A and 3B) were followed by LPP residues, where L374 localised to the adjoining loop that could loosen compactness of these α-helices – this additional flexibility could provide an advantage to this protein that is required for membrane insertion. However, although the environments of α-helices 12 (carrying VMMYL and V-MYL motifs in wild-type and M372del proteins, respectively) were modified in M372del

mutants, these proteins still passed the quality control at the stages of synthesis, topogenesis, folding, and membrane insertion (Fig. 1), but remained dysfunctional (Fig. 2).

As for the loss of transport capacity in M372del mutants (Fig. 2), we suggest that it results from significant changes in properties of α-helices 12 and their interactions in new local environments that could lead to global changes in protein structures (Figs. 3–5). Moreover, residues in VMMYL motifs of wild-type proteins recognised different residues in their vicinity compared to those of V-MYL motifs in M372del mutants (Figs. 3A and 3B). Although, it cannot be excluded that other underlying features may affect the delicate structural balance (not just M372 deletions alone), such as short- and long-range electrostatic interactions and post-translational modifications (specifically phosphorylation sites) around P189 and M372 residues. Concerning regaining the plasma membrane localisation of the P189 M372del mutant, we conclude that the M372 deletion may mitigate the negative effect of a proline substitution in the P189 wild-type protein and provide a structural advantage that results from small (but important) changes in α-helical assembly pathways, collectively leading to the structural compactness. It could also be expected that smaller central cavity volumes in L189, and L189 M372del and P189 M372del proteins contribute to a denser structural packing. This might allow a protein to pass the control mechanisms at the endoplasmic reticulum [55], which detect faulty or aggregated proteins, hence the P189 M372del mutant is delivered to the plasma membrane like the HKT1;5 L189 transporter.

It remains to be addressed in real-time why the P189 variant protein failed to localise to the plasma membrane [8; this work]. Our observations suggest several possibilities: (i) α-helix 6 (carrying P189) cannot form stable intra-helical contacts and/or folds transiently after it emerges from a ribosome; (ii) α-helix 6 does not fold fast enough thus exposes proteolytic sites; (iii) α-helix 6 cannot form an α-hairpin – α-helical folding pair – with a neighbouring α-helix. These α-hairpins play crucial roles as the folding of nuclei in polytopic membrane proteins needs to be completed [46,48]. We postulate that one or a combination of (i-iii) could prevent P189 from passing intracellular control mechanisms, therefore preventing routing to the plasma membrane.

Differences in folding pathways of HKT transporters and their M372del mutants could now be

explored *in vitro* using cell-free synthesis [56] in a bilayer made of a range of lipids [57-59] of allelic variants or truncated and mutated HKTs. It remains to establish if non-functional HvHKT1;5 M372del proteins would maintain stable plasma membrane localisation when expressed in barley using their native promoters, or if membrane proteases would eliminate these functionally unfit proteins to prevent membrane crowding [60]. We also propose that the reconstitution of complex membrane proteins such as HKTs in target membranes could be reliably predicted based on analyses of transmembrane α-helical assembly pathways and MD simulations before experimental investigations are undertaken.

CRediT author contribution

MG, MH, and RW designed the project. SW, JQ, CB, and KH carried out experiments and analysed data. MH performed biocomputational analyses and interpreted data. SW, JQ, and MH prepared Figures and Tables. MH wrote the manuscript with input from all authors. SW, CB, KH, RW, and MG edited the manuscript. All authors commented on the manuscript. We are grateful to the anonymous reviewers for their contribution to the peer review of this work.

Declaration of competing interest

The authors declare that they have no known competing financial interests or personal relationships that could have appeared to influence the work reported in this paper.

Funding sources

SW, JQ, CB, and MG acknowledge funding from the Australian Research Council (CE140100008, DE160100804, and FT180100476). SW and CB thank the Grains Research and Development Corporation for their support. KH and RW acknowledge the Rural & Environment Science & Analytical Services Division of the Scottish Government. MH credits the Huaiyin Normal University (China) for funding.

Legends to Figures

Fig. 1. Transient co-expression of the GFP-HvHKT1;5 L189 variant and its M372del mutant or the HvHKT1;5 P189 variant and its M372del mutant proteins with the RFP-CBL1n plasma membrane marker in *Nicotiana benthamiana* leaf epidermal cells.

(A) L189 variant; (B) P189 variant; (C) L189 M372del mutant; (D) P189 M372del mutant. Left: NH_2-terminally GFP-tagged HvHKT1;5 patterns (green); middle: NH_2-terminally RFP-tagged CBL1n patterns (magenta); right: overlay of both patterns (white). Scale bars = 10 μm. These data were reproducible based on four independent experiments using four different tobacco plants.

Fig. 2. Representative I-V curves of cRNA from HvHKT1;5 L189 and P189, and their M372del mutants injected in *Xenopus laevis* oocytes (n = 4) clamped at -120 mV to 40 mV in Na^+ or K^+ solutions.

(A) L189 variant; (B) P189 variant; (C) L189 M372del mutant; (D) P189 M372del mutant; (E) Control water-injected oocytes. Black circles (1 mM Na^+), black squares (30 mM Na^+), red triangles (30 mM K^+) indicate applied monovalent cations. Note that the y-axis in L189 (panel A) has a different scale compared to those in panels B-E.

Fig. 3. 3D molecular models of HvHKT1;5 L189 and P189 variant and M372del mutant proteins in complex with Na^+.

(A-B) Cylindrical representations of α-helices in L189 and P189 variants (cyan) or their M372del mutants (magenta) illustrate structural features near α-helices 12 (blue and lime in wild-type proteins; grey in M372del mutants). Residues in α-helices 12 in wild-type proteins (motif VMMYL in bold, lime CPK sticks) and M372del mutants (motif V-MYL in bold, grey CPK sticks) face different environments. Separations of less than 3.50 Å of VMMYL or V-MYL residues are shown in dashed lines; interacting residues are labelled in regular text.

(C-left) Superposition (RMSD value of 0.36 Å) of P189 and its M372del mutant shows regions near the selectivity filter. Separations of 2.2-3.4 Å through hexahedral coordination (black dashed

lines) of S78, G233, G353, G457, and Na^+ (grey CPK sticks) are indicated. α-helices 6 carry the P189 variation (yellow CPK sticks) and α-helix 12 (arrow) in P189 M372del contains the V-MYL motif (grey CPK sticks) instead of VMMYL (lime CPK sticks).

(C-middle and right) Superpositions (RMSD value of 0.36 Å) of P189 and its M372del mutant proteins show that the lengths of α-helices 12 differ (arrows).

Fig. 4. Residue fluctuation profile of the HvHKT1;5 L189 and P189 variant proteins.

(A) RMSF plot of protein backbone Cα atoms in L189 (red trace) and P189 (black trace) variant proteins. Disposition of transmembrane α-helices (shown in boxes with H1-H17 designations; not to scale with the x-axis of panel A) that are adjoined by loops (shown as lines) in each structure; numbers above boxes indicate amino acid residues of each α-helix. Horizontal double arrows denote α-helical regions containing L189 or P189 residues on α-helices 6, and VMMYL motifs on α-helices 12. The positions of α-helices 4-6, and α-helices 13 with significantly changed RMSF values between the two structures are also indicated.

(B-left and right) Cylindrical representations of ten superposed models of L189 proteins (left panel) (RMSD values varied between 1.48 Å-1.89 Å) and P189 proteins (right panel) (RMSD values varied between 0.90 Å-1.36 Å). L189 or P189 residues (yellow CPK sticks) are on α-helices 6 (magenta), and VMMYL motifs (cyan CPK sticks) are on α-helices 12. Motions of α-helices 4, 5, and 13 (wheat) have higher fluctuations in L189 proteins than in P189 proteins.

Fig. 5. Residue fluctuation profile of the HvHKT1;5 L189 M372del and P189 M372del mutant proteins.

(A) RMSF plot of protein backbone Cα atoms in L189 M372del (red trace) or P189 M372del (black trace) mutant proteins. The description of disposition of transmembrane α-helices (shown in boxes with H1-H17) is given in Fig. 4. Horizontal double arrows denote α-helical regions containing L189 or P189 residues on α-helices 6, and V-MYL motifs on α-helices 12. The positions of two loops (in the vicinity of α-helices 6 and 12), and α-helices 5, 11, and 13 with significantly changed RMSF values are also indicated.

(B-left and right) Cylindrical representations of ten superposed models of L189 M372del proteins (left panel) (RMSD values varied between 1.21 Å-1.90 Å) or P189 M372del proteins

(right panel) (RMSD values varied between 0.77 Å-1.68 Å). L189 or P189 residues (yellow CPK sticks) are on α-helices 6 (magenta), and V-MYL motifs (cyan CPK sticks) are on α-helices 12. Motions of α-helices 11 and 13, and two loops (adjoining α-helices 9 and 10, and 14 and 15) (wheat) have higher fluctuations in P189 M372del proteins than in L189 M372del proteins.

References

[1] E. Delhaize, W.B. Frommer, M.L. Guerinot, M.J. Harrison, L. Herrera-Estrella, T. Horie, L,V. Kochian, R. Munns, N.K. Nishizawa, Y.F. Tsay, D. Sanders, Using membrane transporters to improve crops for sustainable food production. Nature 497 (2013) 60–66, https://doi.org/10.1038/nature11909.

[2] S.W. Henderson, M. Gilliham, The 'gatekeeper' concept: cell-type specific molecular mechanisms of plant adaptation to abiotic stress. in: R. Laitinen (Ed.), Molecular mechanisms in plant adaptation, Wiley, New York, 2015, pp. 83–116, https://doi.org/10.1002/9781118860526.ch4.

[3] M. Hrmova, M. Gilliham, Plants fighting back: to transport or not to transport, this is a structural question. Curr. Opin. Plant Biol. 46 (2018) 68–76, https://doi.org/10.1016/j.pbi.2018.07.006.

[4] S. Wege, M. Gilliham, S.W. Henderson, Chloride: not simply a 'cheap osmoticum', but a beneficial plant macronutrient. J. Exp. Bot. 68 (2017) 3057–3069, https://doi.org/10.1093/jxb/erx050.

[5] R. Munns, M. Gilliham, Salinity tolerance of crops – what is the cost? New Phytol. 225 (2020) 668–674, https://doi.org/10.1111/nph.13519

[6] R. Munns, D.A. Day, W. Fricke, M. Watt, B. Arsova, B.J. Barkla, J. Bose, C.S. Byrt, Z.H. Chen, K.J. Foster, M. Gilliham, S.W. Henderson, C.L.D. Jenkins, H.J. Kronzucker, S.J. Miklavcic, D. Plett, S.J. Roy, S. Shabala, M.C. Shelden, K.L. Soole, N.L. Taylor, M. Tester, S. Wege, L.H. Wegner, S.D. Tyerman, Energy costs of salt tolerance in crop plants. New Phytol. 208 (2015) 1072–1090, https://doi.org/10.1111/nph.15864.

[7] S. Somasundaram, A.A. Véry, R.S. Vinekar, T. Ishikawa, K. Kumari, S. Pulipati, K. Kumaresan, C. Corratgé-Faillie, R. Sowdhamini, A. Parida, L. Shabala, S. Shabala, G.

Venkataraman, Homology modeling identifies crucial amino-acid residues that confer higher Na^+ transport capacity of OcHKT1;5 from *Oryza coarctata* Roxb. Plant Cell Physiol. 61 (2020) 1321–1334, https://doi.org/10.1093/pcp/pcaa061.

[8] K. Houston, J. Qiu, S. Wege, M. Hrmova, H. Oakey, Y. Qu, P. Smith, A. Situmorang, M. Macaulay, P. Flis, M. Bayer, C. Halpin, S. Roy, J. Russell, C. Byrt, M.J. Gilliham, D.E. Salt, R. Waugh, Barley sodium content is regulated by natural variants of the Na^+ transporter HvHKT1;5. Commun. Biol. 3 (2020) 258, https://doi.org/10.1038/s42003-020-0990-5.

[9] J.G. Almeida, A.J. Preto, P.I. Koukos, A.M.J.J. Bonvin, I.S. Moreira, Membrane proteins structures: a review on computational modeling tools. Biochim. Biophys. Acta 1859 (2017) 2021–2039, https://doi.org/10.1016/j.bbamem.2017.07.008.

[10] D. Rakesh, C. Byrt, S.D. Tyerman, M. Gilliham, S. Wege, Roles of membrane transporters: connecting the dots from sequence to phenotype, Ann. Bot. 124 (2019) 201–208, https://doi.org/10.1093/aob/mcz066.

[11] S.R. Durell, H.R. Guy, Structural models of the KtrB, TrkH, and Trk1,2 symporters based on the structure of the KcsA K^+ channel. Biophys. J. 77 (1999) 789–807, https://doi.org/10.1016/S0006-3495(99)76932-8.

[12] C. Corratgé-Faillie, M. Jabnoune, S. Zimmermann, A.A. Véry, C. Fizames, H. Sentenac, Potassium and sodium transport in non-animal cells: The Trk/Ktr/HKT transporter family. Cell. Mol. Life Sci. 67 (2010) 2511–2532, https://doi.org/10.1007/s00018-010-0317-7.

[13] M.H. Saier, V.S. Reddy, B.V. Tsu, M.S. Ahmed, C. Chun Li, G. Moreno-Hagelsieb, The Transporter Classification Database (TCDB): recent advances. Nucleic Acids Res. 44 (2016) D372–D379, https://doi.org/10.1093/nar/gkv1103.

[14] Y. Cao, X. Jin, H. Huang, M.G. Derebe, E.J. Levin, V. Kabaleeswaran, Y. Pan, M. Punta, J. Love, J. Weng, Crystal structure of a potassium ion transporter. TrkH. Nature 471 (2011) 336–340, https://doi.org/10.1038/nature09731.

[15] O. Cotsaftis, D. Plett, N. Shirley, M. Tester, M. Hrmova, A two-staged model of Na^+ exclusion in rice explained by 3D modeling of HKT transporters and alternative splicing. PLoS ONE 7 (2012) e39865, https://doi.org/10.1371/journal.pone.0039865.

[16] R.S. Vieira-Pires, A. Szollosi, J.H. Morais-Cabral, The structure of the KtrAB potassium transporter. Nature 496 (2012) 323–328, https://doi.org/10.1038/nature12055.

[17] J.D. Platten, O. Cotsaftis, P. Berthomieu, H. Bohnert, R.J. Davenport, D.J. Fairbairn, T. Horie, R.A. Leigh, H.X. Lin, S. Luan, P. Mäser, O. Pantoja, A. Rodríguez-Navarro, D.P. Schachtman, J.I. Schroeder, H. Sentenac, N. Uozumi, A.A. Véry, J.K. Zhu, E.S. Dennis, M. Tester, Nomenclature for HKT transporters, key determinants of plant salinity tolerance. Trends Plant Sci. 11 (2006) 372–374, https://doi.org/10.1016/j.tplants.2006.06.001.

[18] T. Horie, F. Hauser, J.I. Schroeder, HKT transporter-mediated salinity resistance mechanisms in Arabidopsis and monocot crop plants. Trends Plant Sci. 14 (2009) 660–668, https://doi.org/10.1016/j.tplants.2009.08.009.

[19] S. Waters, M. Gilliham, M. Hrmova, Plant high affinity potassium (HKT) transporters involved in salinity tolerance: structural insights to probe differences in ion selectivity. Int. J. Mol. Sci. 14 (2013) 7660–7680, https://doi.org/10.3390/ijms14047660.

[20] W.-Z. Lan, W. Wang, S.-M. Wang, Y.-G. Li, B.B. Buchanan, H.-X. Lin, J.-P. Gao, S. Luan, A rice high-affinity potassium transporter (HKT) conceals a calcium-permeable cation channel. Proc. Natl. Acad. Sci. U. S. A. 107 (2010) 7089–7094, https://doi.org/10.1073/pnas.1000698107.

[21] T. Horie, D.E. Brodsky, DA. Costa, T. Kaneko, F. Lo Schiavo, M. Katsuhara, J.I. Schroeder, K^+ transport by the OsHKT2;4 transporter from rice with atypical Na^+ transport properties and competition in permeation of K^+ over Mg^{2+} and Ca^{2+} ions. Plant Physiol. 156 (2011) 1493–1507, https://doi.org/10.1104/pp.110.168047.

[22] D. Plett, G. Safwat, M. Gilliham, I. Skrumsager Møller, S. Roy, N. Shirley, A. Jacobs, A. Johnson, M. Tester, Salinity tolerance of rice through cell type-specific expression of AtHKT1;1. PLoS ONE 5 (2010) e12571, https://doi.org/10.1371/journal.pone.0012571.

[23] R.J. Munns, R.A. James, B. Xu, A. Athman, S.J. Conn, C. Jordans, C.S. Byrt, R.A. Hare, S.D. Tyerman, M. Tester, D. Plett, M. Gilliham, Wheat grain yield on saline soils is improved by an ancestral Na^+ transporter gene. Nat. Biotechnol. 30 (2012) 360–364, https://doi.org/10.1038/nbt.2120.

[24] B. Xu, S. Waters, C.S. Byrt, D. Plett, S.D, Tyerman, M. Tester, R. Munns, M. Hrmova, M. Gilliham, Structural variations in wheat HKT1;5 underpin differences in Na^+ transport capacity. Cell. Mol. Life Sci. 75 (2018) 1133–1144, https://doi.org/10.1007/s00018-017-2716-5.

[25] C. Borjigin, R.K. Schilling, J. Bose, M. Hrmova, J. Qiu, S. Wege, A. Situmorang, C. Byrt, C. Brien, B. Berger, M. Gilliham, A.S. Pearson, S.J. Roy, A single nucleotide substitution in TaHKT1;5-D controls shoot Na^+ accumulation in bread wheat. Plant Cell Environ. 43 (2020) 2158–2171, https://doi.org/10.1111/pce.13841.

[26] B. Xu, M. Hrmova, M. Gilliham, High affinity Na^+ transport by wheat HKT1;5 is blocked by K^+. Plant Direct 4(10) (2020) e00275, https://doi.org/10.1002/pld3.275.

[27] M. Gilliham, J. Able, S. Roy, Translating knowledge about abiotic stress tolerance to breeding programmes. Plant J. 90 (2017) 98–917, https://doi.org/10.1111/tpj.13456.

[28] G. Celniker, G. Nimrod, H. Ashkenazy, F. Glaser, E. Martz, I. Mayrose, T. Pupko, N. Ben-Tal, ConSurf: Using evolutionary data to raise testable hypotheses about protein function. Isr. J. Chem. 53 (2013) 199–206, https://doi.org/10.1002/ijch.201200096.

[29] T. L. Bailey, M. Bodén, F. A. Buske, M. Frith, C. E. Grant, L. Clementi, J. Ren, W. W. Li, W. S. Noble, MEME SUITE: tools for motif discovery and searching. Nucleic Acids Res. 37 (2009) W202–W208, https://doi.org/10.1093/nar/gkp335.

[30] F. Sievers, A. Wilm, D. Dineen, T. J. Gibson, K. Karplus, W. Li, R. Lopez, H. McWilliam, M. Remmert, J. Söding, J.D. Thompson, D. G. Higgins, Fast, scalable generation of high-quality protein multiple sequence alignments using Clustal Omega. Mol. Syst. Biol. 7 (2011) 539–548, https://doi.org/10.1038/msb.2011.75.

[31] J. Pei, B.-H. Kim, N.V. Grishin, PROMALS3D: a tool for multiple protein sequence and structure alignments. Nucleic Acids Res. 36 (2008) 2295–2300, https://doi.org/10.1093/nar/gkn072.

[32] Y. Wu, S.W. Henderson, S. Wege, F. Zheng, A.R. Walker, R.R. Walker, M. Gilliham, The grapevine *NaE* sodium exclusion locus encodes sodium transporters with diverse transport properties and localisation. J. Plant Physiol. 247 (2020) 153113, https://doi.org/10.1016/j.jplph.2020.153113.

[33] O. Batistič, N. Sorek, S. Schultke, S. Yalovsky, J. Kudla, Dual fatty acyl modification determines the localization and plasma membrane targeting of CBL/CIPK Ca^{2+} signaling complexes in Arabidopsis. Plant Cell 20 (2008) 1346–1362, https://doi.org/10.1105/tpc.108.058123.

[34] C.A. Schneider, W.S. Rasband, K.W. Eliceiri, NIH Image to ImageJ: 25 years of image analysis. Nat. Methods 9 (2012) 671–675, https://doi.org/10.1038/nmeth.2089.

[35] C. Byrt, B. Xu M. Krishnan, D.J. Lightfoot, A. Athman, A.K. Jacobs, N.S. Watson- Haigh, D. Plett, R. Munns, M. Tester, M. Gilliham, The Na^+ transporter, TaHKT1;5-D, limits shoot Na^+ accumulation in bread wheat. Plant J. 80 (2014) 516–526, https://doi.org/10.1111/tpj.12651.

[36] D. Beglov, B. Roux, Finite representation of an infinite bulk system: Solvent boundary potential for computer simulations. J. Chem. Phys. 100 (1994) 9050–9063, https://doi.org/10.1063/1.466711.

[37] B.R. Brooks, C.L. Brooks 3rd, A.D. Mackerell Jr, L. Nilsson, R.J. Petrella, B. Roux, Y. Won, G. Archontis, C. Bartels, S. Boresch, A. Caflisch, L. Caves, D. Cui, A.R. Dinner, M. Feig, S. Fischer, J. Gao, M. Hodoscek, W. Im, K. Kuczera, T. Lazaridis, J. Ma, V. Ovchinnikov, E. Paci, R.W. Pastor, C.B. Post, J.Z. Pu, M. Schaefer, B. Tidor, R.M. Venable, H.L. Woodcock, X. Wu, W. Yang, D.M. York, M. Karplus, CHARMM: The Biomolecular Simulation Program. J. Comp. Chem. 30 (2009) 1545–1615, https://doi.org/10.1002/jcc.21287.

[38] Šali, T. Blundell, Comparative protein modeling by satisfaction of spatial restraints. J. Mol. Biol. 234 (1993) 779–815, https://doi.org/10.1006/jmbi.1993.1626.

[39] M.Y. Shen, A. Šali, Statistical potential for assessment and prediction of protein structures. Protein Sci. 15 (2006) 2507–2524, https://doi.org/10.1110/ps.062416606.

[40] N. Eswar, D. Eramian, B. Webb, M.Y. Shen, A. Šali, Protein structure modeling with Modeller, in: B. Kobe, M. Guss, T. Huber (Eds.), Structural proteomics, Humana Press, Totowa, 2008, pp. 145–159.

[41] R.A. Laskowski, M.W. MacArthur, D.S. Moss, J.M. Thornton, PROCHECK: a program to check the stereochemical quality of protein structures. J. App. Crystallogr. 26 (1993) 283–291, https://doi.org/10.1107/S0021889892009944.

[42] M.J. Sippl, Recognition of errors in three-dimensional structures of proteins. Proteins 17 (1993) 355–362, https://doi.org/10.1002/prot.340170404.

[43] P. Benkert, M. Biasini, T. Schwede, Toward the estimation of the absolute quality of individual protein structure models. Bioinformatics 27 (2011) 343–350, https://doi.org/10.1093/bioinformatics/btq662.

[44] J.W.H. Schymkowitz, F. Rousseau, I.C. Martins, J. Ferkinghoff-Borg, F. Stricher, L. Serrano, Prediction of water and metal binding sites and their affinities by using the Fold-X force field. Proc. Natl. Acad. Sci. U. S. A. 102 (2005) 10147–10152, https://doi.org/10.1073/pnas.0501980102.

[45] W. Tian, C. Chen, X. Lei, J. Zhao, J. Liang. CASTp 3.0: computed atlas of surface topography of proteins. Nucleic Acids Res. 46 (2018) W363–W367, https://doi.org/10.1093/nar/gky473.

[46] A.L. Lomize, K.A. Schnitzer, I.D. Pogozheva, TMPfold: A web tool for predicting stability of transmembrane α-helix association. J. Mol. Biol. (2020) 432, 3388–3394, https://doi.org/10.1016/j.jmb.2019.10.024.

[47] L. Kall, A. Krogh, E.L. Sonnhammer, An HMM posterior decoder for sequence feature prediction that includes homology information. Bioinformatics 21 (2005) i251–i257, https://doi.org/10.1093/bioinformatics/bti1014.

[48] H. Yu, M.G.W. Siewny, E.T. Edwards, A.W. Sanders, T.T. Perkins, Hidden dynamics in the unfolding of individual bacteriorhodopsin proteins. Science 355 (2017) 945–950, http://science.sciencemag.org/content/355/6328/945.

[49] Kuriata, A.M. Gierut, T. Oleniecki, M.P. Ciemny, A. Kolinski, M. Kurcinski, S. Kmiecik, CABS-flex 2.0: a web server for fast simulations of flexibility of protein structures. Nucleic Acids Res. 46 (2018) W338–W343, https://doi.org/10.1093/nar/gky356.

[50] R. Guo, Z. Cang, J. Yao, M. Kim, E. Deans, G. Wei, S.-G. Kang, H. Hong, Structural cavities are critical to balancing stability and activity of a membrane-integral enzyme.

Proc. Natl. Acad. Sci. U. S. A. 117 (2020) 22146–22156, https://doi.org/10.1073/pnas.1917770117.

[51] E. Mercier, W. Wintermeyer, M.V. Rodnina, Co-translational insertion and topogenesis of bacterial membrane proteins monitored in real time. EMBO J. 39 (2020) e104054, https://doi.org/10.15252/embj.2019104054.

[52] T.W. Kim, S.G. Lee, J. Jo, J.G. Kim, H. Ki, S.W. Kim, K.H. Cho, J. Choi, J.H. Lee, M. Wulff, Y.M. Rhee, H. Ihee, Protein folding from heterogeneous unfolded state revealed by time-resolved X-ray solution scattering. Proc. Natl. Acad. Sci. U. S. A. 117 (2020) 14996–15005, https://doi.org/10.1073/pnas.1913442117.

[53] T. Pleiner, G.P. Tomaleri, K. Januszyk, A.J. Inglis, M. Hazu, R.M. Voorhees, Structural basis for membrane insertion by the human ER membrane protein complex. Science 369 (2020) 433–436, https://doi.org/10.1126/science.abb5008.

[54] N.J. Harris, E. Reading, K. Ataka, L. Grzegorzewski, K. Charalambous, X. Liu, R. Schlesinger, J. Heberle, P.J. Booth, Structure formation during translocon-unassisted co-translational membrane protein folding. Sci. Rep. 7 (2017) 8021, https://doi.org/10.1038/s41598-017-08522-9.

[55] K. Zhang, R.J Kaufman, Signaling the unfolded protein response from the endoplasmic reticulum. J. Biol. Chem. 279 (2004) 25935–25938, https://doi.org/10.1074/jbc.R400008200.

[56] N. Shadiac, Y. Nagarajan, S. Waters, M. Hrmova, The close allies in membrane protein research: cell-free synthesis and nanotechnology. Mol. Membr. Biol. 30 (2013) 229–245, https://doi.org/10.3109/09687688.2012.762125.

[57] Y. Nagarajan, J. Rongala, S. Luang, A. Sing, N. Shadiac, J. Hayes, T. Sutton, M. Gilliham, S.D. Tyerman, G. McPhee, N.H. Voelcker, H.D.T. Mertens, N.M. Kirby, J.-G. Lee, Y.G. Yingling, M. Hrmova, A barley efflux transporter operates in a Na^+-dependent manner, as revealed through a multidisciplinary platform. Plant Cell 28 (2016) 202–218, https://doi.org/10.1105/tpc.15.00625.

[58] N.J. Harris, G.A. Pellowe, P.J. Booth, Cell-free expression tools to study co-translational folding of alpha helical membrane transporters. Sci. Rep. 10 (2020) 9125, https://doi.org/10.1038/s41598-020-66097-4.

[59] 4j7cP. Pettersson, J. Patrick, M. Jakob, M. Jacobs, R. B. Klösgen, S. Wennmalm, L. Mäler, Soluble TatA forms oligomers that interact with membranes: Structure and insertion studies of a versatile protein transporter. Biochim. Biophys. Acta - Biomembranes 1863 (2021) 183529, https://doi.org/10.1016/j.bbamem.2020.183529

[60] K. Strisovski, Why cells need intramembrane proteases – a mechanistic perspective. FEBS J. 283 (2015) 1837–1845, https://doi.org/10.1111/febs.13638.

Table 1. Predicted transmembrane α-helical assembly pathways of HvHKT1;5 L189, L189M 372del, and P189, P189 M372del and L189P, and KtrB K^+ transporters during co-translational protein folding.

Haplotype	**HvHKT1;5**	**Assembly pathway** [a, b]
Na^+_{HAP1}	L189	(((1+2)+(3+4))+5),((((**6**+7)+8)+9)+(10+11)),((((**12**+13)+14)+15)+(16+17))
	L189 M372del	((1+2)+(3+4)),(5+(((**6**+7)+8)+9)),((((10+11)+**12**)+(13+(14+15)))+(16+17))
Na^+_{HAP3}	P189	(((((1+2)+(3+4))+5)+((**6**+7)+8))+((9+((((10+11)+**12**)+13)+(14+15)))+(16+17)))
	P189 M372del	(((((1+2)+(3+4))+5)+(((**6**+7)+8)+9))+(((10+11)+**12**)+(13+(((14+15)+16)+17))))
	P189L	((1+2)+(3+4)),(5+(((**6**+7)+8)+9)),((((10+11)+**12**)+(13+(14+15)))+(16+17))
	KtrB K^+	((((1+2)+(3+4))+5)+(6+7)),((((8+9)+(10+11))+12)+13),((14+15)+(16+17))

[a] L189 and P189 residues are on α-helices 8, and VMMYL and V-MYL (M372del of VMMYL) motifs are on α-helices **12**.

[b] Sequences of α-helices 12: L189 and P189 (SAVVVVYMVMMYL); L189 and P189 M372del (SAVVVVYMVMY).

Table 2.

Summary of properties of HvHKT1;5 L189 and L189 M372del, and P189 and P189 M372del transporters in complex with Na^+.

Haplotype	HvHKT1;5	Plasma membrane localisation	Na^+/K^+ transport	Predicted structural disruptions in: /molecular shape /angle of α-helix 6 [a] /length of α-helix 12 [a] /interactions of residues in α-helix 12 [a] /α-helical assembly pathway [a]
Na^+_{HAP1}	L189	+	+	- /- /- /-/in 3 events via 14 steps
	L189M372del	+	-	- /- /+ /-/in 3 events via 14 steps
Na^+_{HAP3}	P189	-	N.A. [b]	+ /+ /- /-/in 1 event via 16 steps
	P189M372del	+	-	- /+ /+ /+/in 1 event via 16 steps

[a] L189 and P189 residues are on α-helices **6**, and V-MYL and V-MYL motifs on α-helices **12**.

[b] N.A. indicates not applicable, as the P189 protein did not localise to the plasma membrane.

Graphical abstract

Highlights

- HvHKT1;5 transporters contribute to salinity tolerance of major cereal crops
- M372 deletion in HvHKT1;5 P189 restores plasma membrane localisation but not conductance
- 3D models and α-helical assembly pathways of HKT mutants rationalise protein folding
- M372 deletion causes changes in flexibility of α-helices and loops in HvHKT1;5 mutants

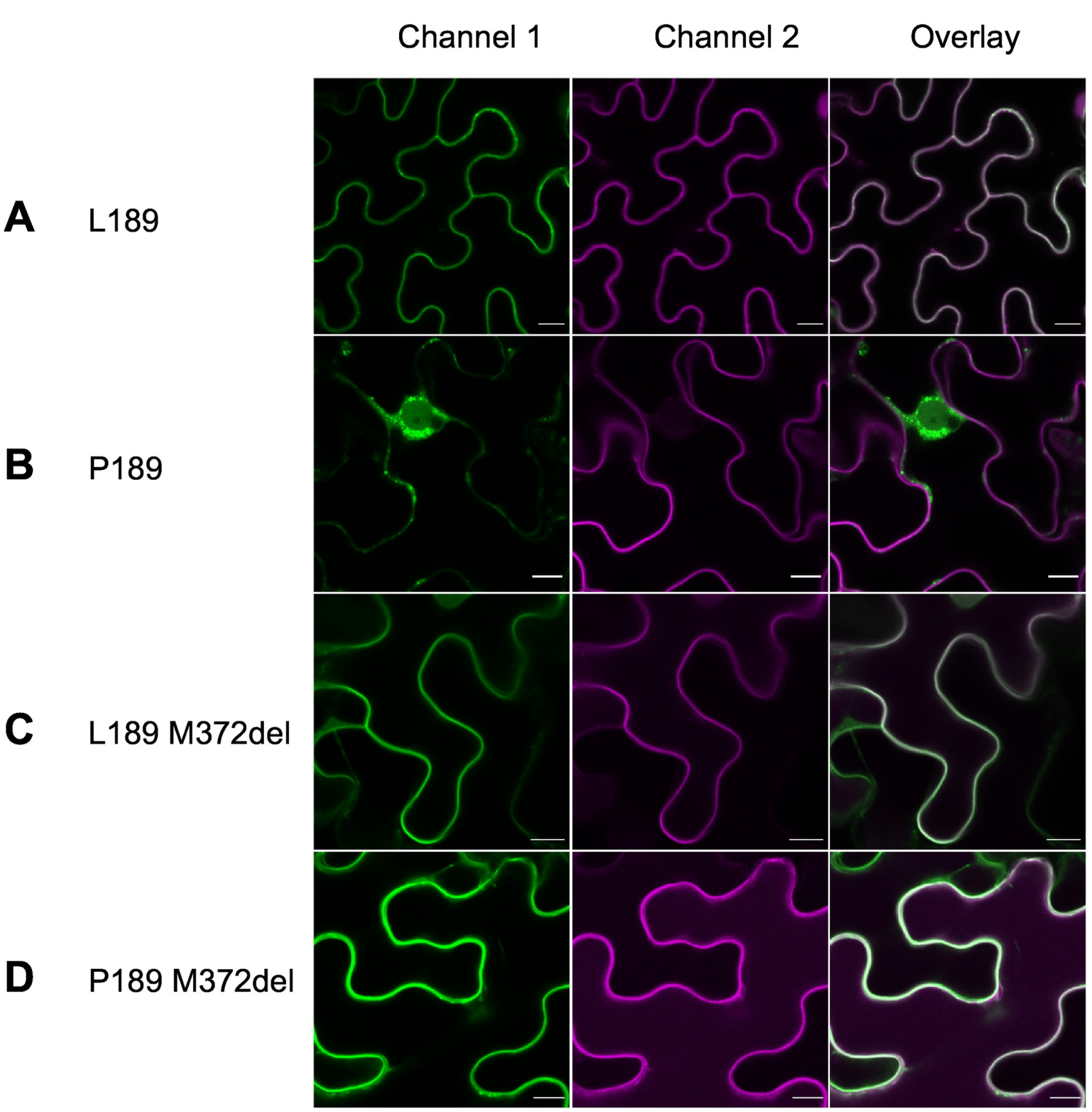
Channel 1
Channel 2
Overlay
A
L189
B
P189
C
L189 M372del
D
P189 M372del

Figure 1

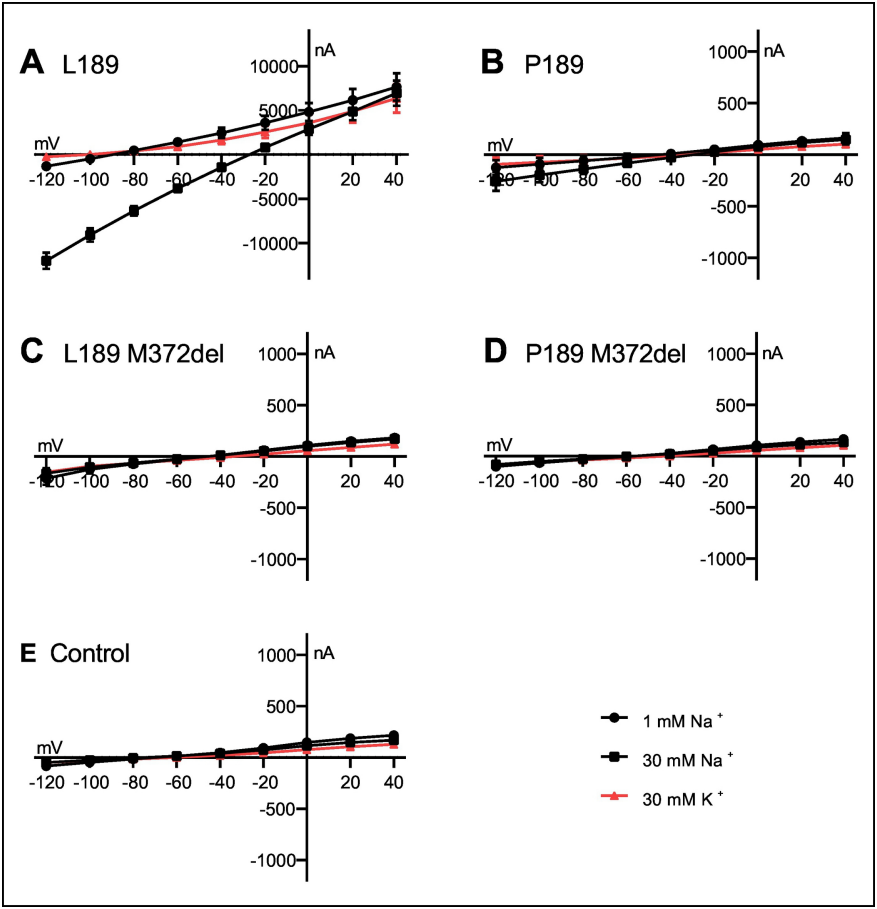
A L189
nA
10000
5000
mV
-120 -100 -80 -60 -40 -20 20 40
-5000
-10000
B P189
1000
nA
500
mV
-120 -100 -80 -60 -40 -20 20 40
-500
-1000
C L189 M372del
1000
nA
500
mV
-120 -100 -80 -60 -40 -20 20 40
-500
-1000
D P189 M372del
1000
nA
500
mV
-120 -100 -80 -60 -40 -20 20 40
-500
-1000
E Control
1000
nA
500
mV
-120 -100 -80 -60 -40 -20 20 40
-500
-1000
1 mM Na +
30 mM Na +
30 mM K +

Figure 2

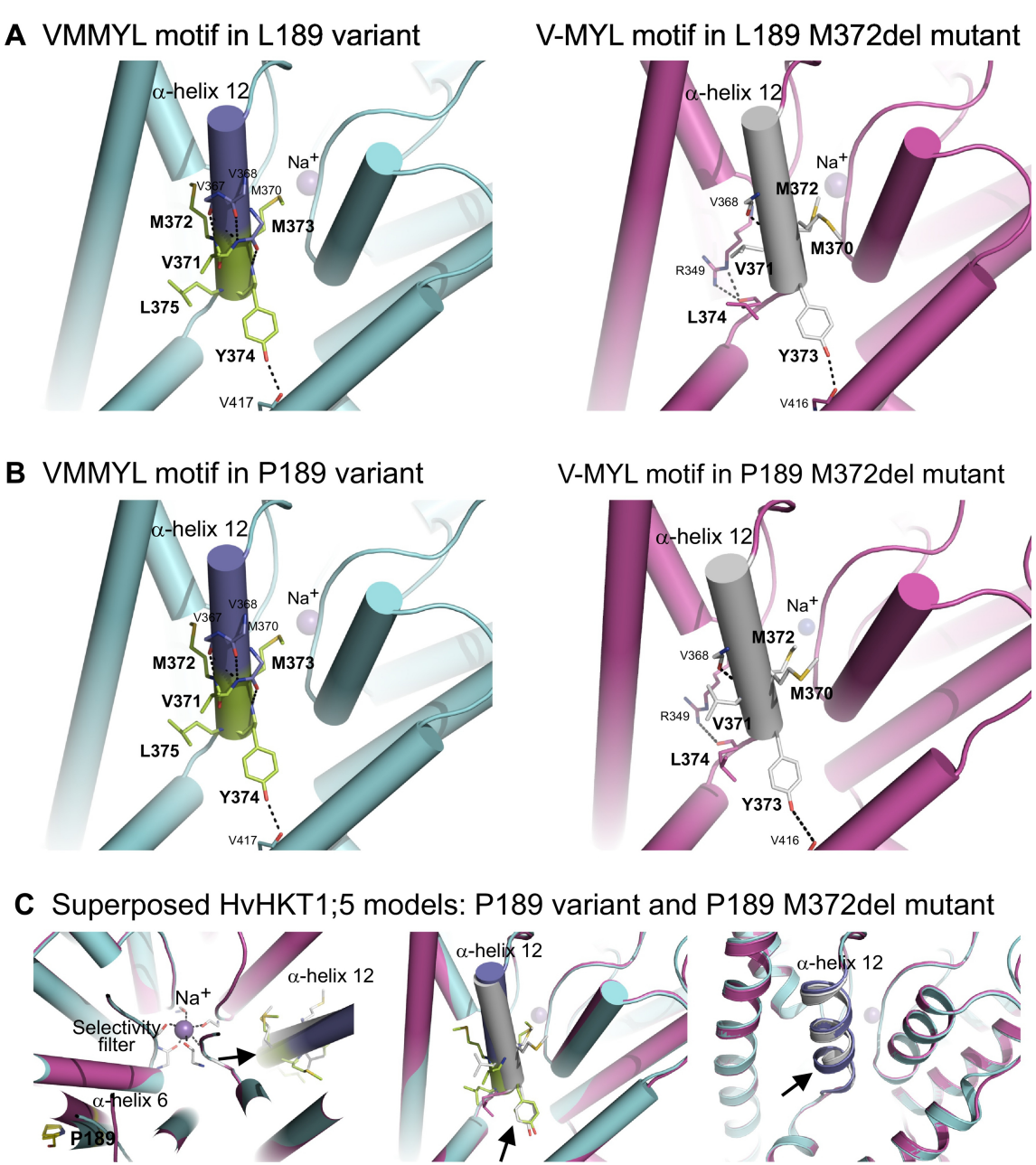
A VMMYL motif in L189 variant
α-helix 12
Na+
V368
V367
M370
M372
M373
V371
L375
Y374
V417
V-MYL motif in L189 M372del mutant
α-helix 12
Na+
M372
V368
M370
R349
V371
L374
Y373
V416
B VMMYL motif in P189 variant
α-helix 12
Na+
V368
V367
M370
M372
M373
V371
L375
Y374
V417
V-MYL motif in P189 M372del mutant
α-helix 12
Na+
M372
V368
M370
R349
V371
L374
Y373
V416
C Superposed HvHKT1;5 models: P189 variant and P189 M372del mutant
Na+
α-helix 12
Selectivity filter
α-helix 6
P189
α-helix 12
α-helix 12

Figure 3

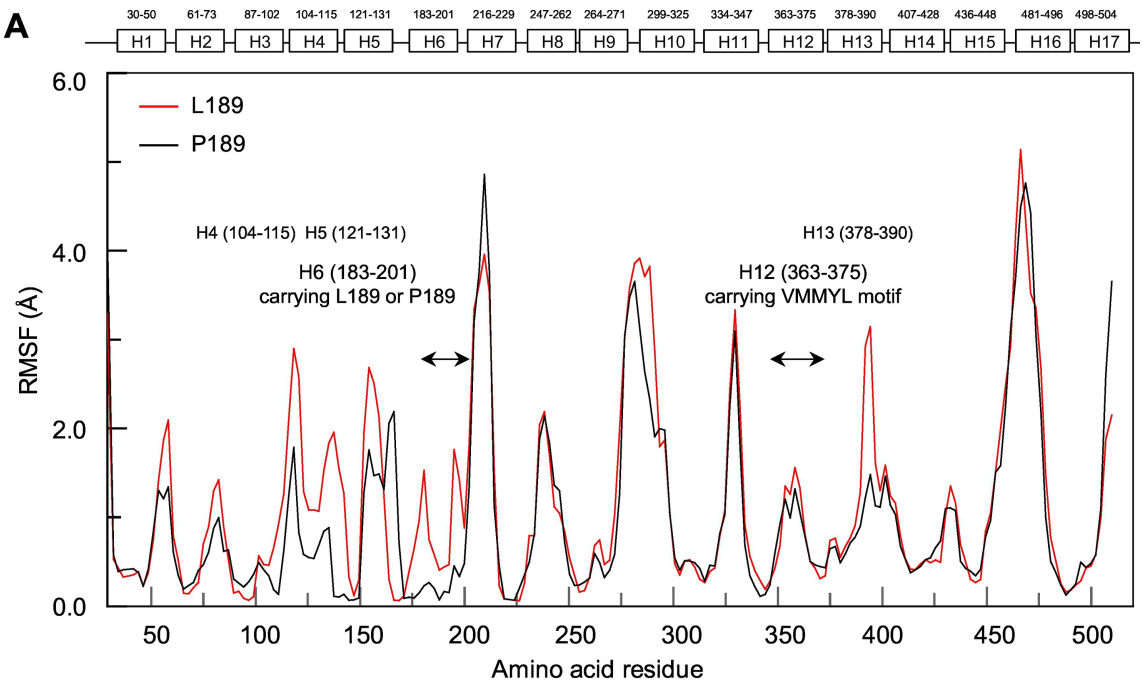
A
30-50
61-73
87-102
104-115
121-131
183-201
216-229
247-262
264-271
299-325
334-347
363-375
378-390
407-428
436-448
481-496
498-504
H1
H2
H3
H4
H5
H6
H7
H8
H9
H10
H11
H12
H13
H14
H15
H16
H17
L189
P189
H4 (104-115) H5 (121-131)
H6 (183-201)
carrying L189 or P189
H13 (378-390)
H12 (363-375)
carrying VMMYL motif
RMSF (Å)
6.0
4.0
2.0
0.0
50
100
150
200
250
300
350
400
450
500
Amino acid residue

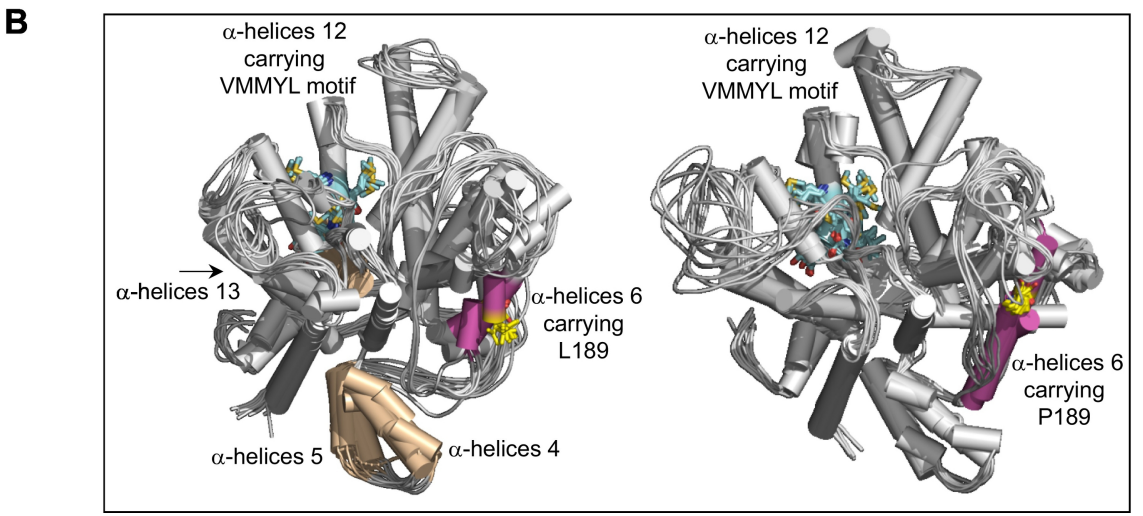
B
α-helices 12
carrying
VMMYL motif
α-helices 13
α-helices 6
carrying
L189
α-helices 5
α-helices 4
α-helices 12
carrying
VMMYL motif
α-helices 6
carrying
P189

Figure 4

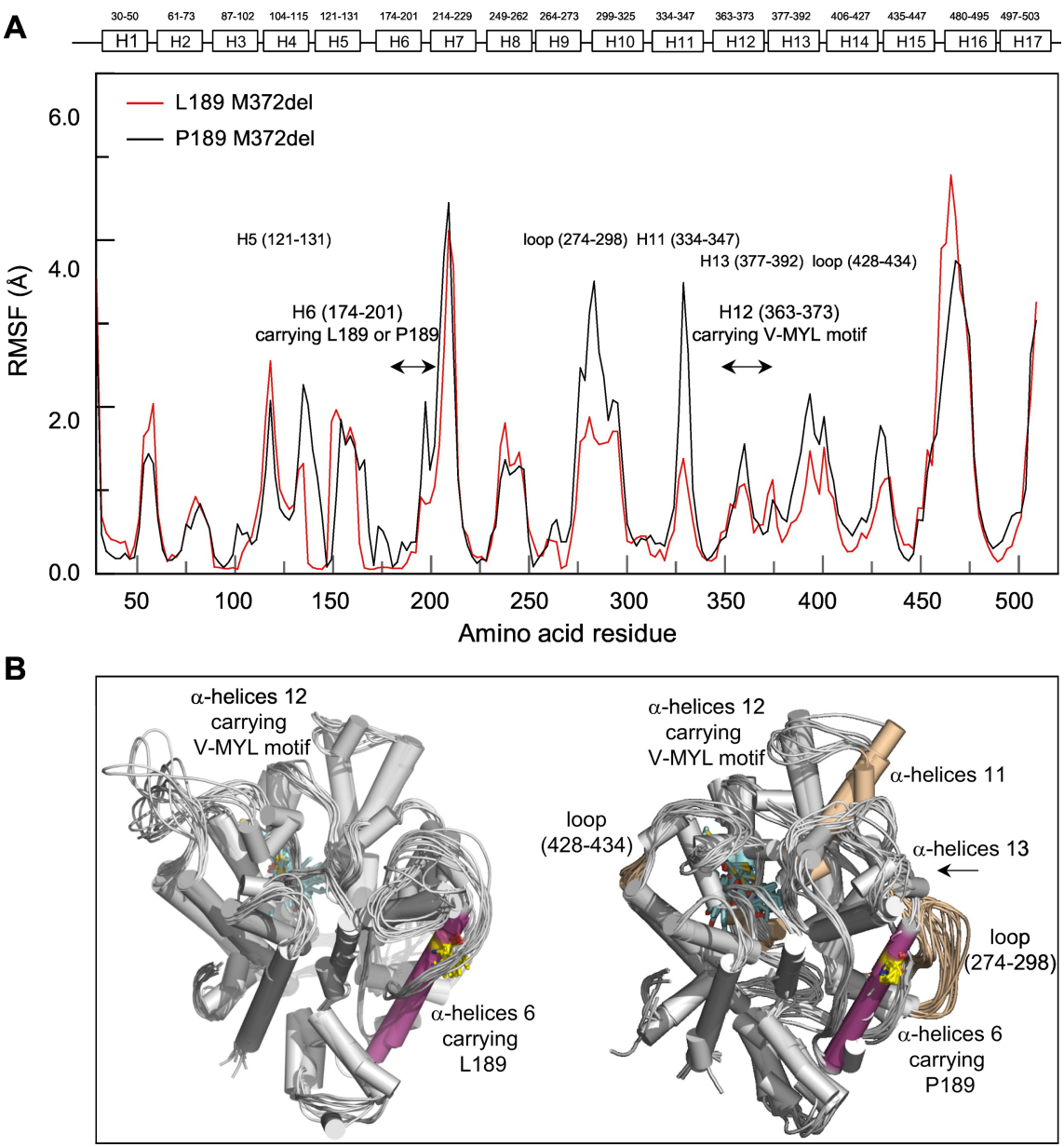
A
30-50
61-73
87-102
104-115
121-131
174-201
214-229
249-262
264-273
299-325
334-347
363-373
377-392
406-427
435-447
480-495
497-503
H1
H2
H3
H4
H5
H6
H7
H8
H9
H10
H11
H12
H13
H14
H15
H16
H17
L189 M372del
P189 M372del
RMSF (Å)
6.0
4.0
2.0
0.0
H5 (121-131)
H6 (174-201)
carrying L189 or P189
loop (274-298) H11 (334-347)
H13 (377-392) loop (428-434)
H12 (363-373)
carrying V-MYL motif
50
100
150
200
250
300
350
400
450
500
Amino acid residue
B
α-helices 12
carrying
V-MYL motif
α-helices 6
carrying
L189
α-helices 12
carrying
V-MYL motif
α-helices 11
loop
(428-434)
α-helices 13
loop
(274-298)
α-helices 6
carrying
P189

Figure 5